# A fair comparison between ultrathin crystalline-silicon solar cells with either periodic or correlated disorder inverted pyramid textures

Muller, Jérôme; Herman, Aline; Mayer, Alexandre; Deparis, Olivier

*Published in:*
Optics Express

*DOI:*
10.1364/OE.23.00A657

*Publication date:*
2015

*Document Version*
Early version, also known as pre-print

# A fair comparison between ultrathin crystalline-silicon solar cells with either periodic or correlated disorder inverted pyramid textures

**Jérôme Muller,* Aline Herman, Alexandre Mayer, and Olivier Deparis**

*Research Center in Physics of Matter and Radiation (PMR), Department of Physics, University of Namur, 61 rue de Bruxelles, B-5000 Namur, Belgium*

*jerome.muller@unamur.be

**Abstract:** Fabrication of competitive solar cells based on nano-textured ultrathin silicon technology is challenging nowadays. Attention is paid to the optimization of this type of texture, with a lot of simulation and experimental results published in the last few years. While previous studies discussed mainly the local features of the surface texture, we highlight here the importance of their filling fraction. In this work, we focus on a fair comparison between a technologically realizable correlated disorder pattern of inverted nano-pyramids on an ultrathin crystalline-silicon layer, and its periodically patterned counterpart. A fair comparison is made possible by defining an equivalent periodic structure for each hole filling fraction. Moreover, in order to be as realistic as possible, we consider patterns that could be fabricated by standard patterning techniques: hole-mask colloidal lithography, nanoimprint lithography and wet chemical etching. Based on numerical simulations, we show that inverted nano-pyramid patterns with correlated disorder provide typically greater efficiency than their periodic counterparts. However, the hole filling fraction of the etched pattern plays a crucial role and may limit the benefits of the correlated disorder due to experimental restrictions on pattern fabrication.



**OCIS codes:** (350.6050) Solar energy; (310.6628) Subwavelength structures, nanostructures; (310.6845) Thin film devices and applications; (000.3860) Mathematical methods in physics.

## References and links

1. R. Singh, "Why silicon is and will remain the dominant photovoltaic material," J. Nanophoton. **3**, 032503 (2009).
2. European Photovoltaic Industry Association, `www.epia.org` (2015).
3. M. A. Green, "Third generation photovoltaics: Ultra-high conversion efficiency at low cost," Progr. Photovolt. Res. Appl. **9**, 123–135 (2001).
4. International Technology Roadmap for Photovoltaic (ITRPV), http://www.itrpv.net/ (2015).
5. L. Tsakalakos, *Nanotechnology for Photovoltaics* (CRC Press, 2010).
6. J. Nelson, *The Physics of Solar Cells* (Imperial College, 2003).
7. P. Campbell and M. A. Green, "Light trapping properties of pyramidally textured surfaces," J. Appl. Phys. **62**, 243–249 (1987).
8. E. Yablonovitch and G. Cody, "Intensity enhancement in textured optical sheets for solar cells," IEEE Trans. Electron. Dev. **29**, 300–305 (1982).
9. A. Bozzola, M. Liscidini, and L. C. Andreani, "Photonic light-trapping versus lambertian limits in thin film silicon solar cells with 1D and 2D periodic patterns," Opt. Express **20**, A224–A244 (2012).

#235598 - $15.00 USD Received 4 Mar 2015; revised 22 Apr 2015; accepted 26 Apr 2015; published 15 May 2015

10. M. M. de Jong, P. J. Sonneveld, J. Baggerman, C. J. M. van Rijn, J. K. Rath, and R. E. I. Schropp, "Utilization of geometric light trapping in thin film silicon solar cells: simulations and experiments," Prog. Photovolt. Res. Appl. **22**, 540–547 (2014).
11. L. C. Andreani, A. Bozzola, P. Kowalczewski, and M. Liscidini, "Photonic light trapping and electrical transport in thin-film silicon solar cells," Sol. Energy Mater. Sol. Cells **135**, 78–92 (2015).
12. R. Rothemund, T. Umundum, G. Meinhardt, K. Hingerl, T. Fromherz, and W. Jantsch, "Light trapping in pyramidally textured crystalline silicon solar cells using back-side diffractive gratings," Prog. Photovolt. Res. Appl. **21**, 747–753 (2013).
13. D. Zhou, Y. Pennec, B. Djafari-Rouhani, O. Cristini-Robbe, T. Xu, Y. Lambert, Y. Deblock, M. Faucher, and D. Stivenard, "Optimization of the optical properties of nanostructured silicon surfaces for solar cell applications," J. Appl. Phys. **115**, 134304 (2014).
14. C. Battaglia, C.-M. Hsu, K. Söderström, J. Escarré, F.-J. Haug, M. Charrière, M. Boccard, M. Despeisse, D. T. L. Alexander, M. Cantoni, Y. Cui, and C. Ballif, "Light trapping in solar cells: Can periodic beat random," ACS Nano **6**, 2790–2797 (2012).
15. M. Peters, K. Forberich, C. Battaglia, A. G. Aberle, and B. Bläsi, "Comparison of periodic and random structures for scattering in thin-film microcrystalline silicon solar cells," in *Proc. SPIE*, vol. 8438 (Brussels, Belgium, 2012), vol. 8438, p. 84380F.
16. H. Fredriksson, Y. Alaverdyan, A. Dmitriev, C. Langhammer, D. Sutherland, M. Zäch, and B. Kasemo, "Hole-mask colloidal lithography," Adv. Mater. **19**, 4297–4302 (2007).
17. A. Oskooi, P. A. Favuzzi, Y. Tanaka, H. Shigeta, Y. Kawakami, and S. Noda, "Partially disordered photonic-crystal thin films for enhanced and robust photovoltaics," Appl. Phys. Lett. **100**, 181110 (2012).
18. R. Peretti, G. Gomard, L. Lalouat, C. Seassal, and E. Drouard, "Absorption control in pseudodisordered photonic-crystal thin films," Phys. Rev. A **88**, 053835 (2013).
19. A. Bozzola, M. Liscidini, and L. C. Andreani, "Broadband light trapping with disordered photonic structures in thin-film silicon solar cells," Prog. Photovolt. Res. Appl. **22**, 1237–1245 (2014).
20. E. R. Martins, J. Li, Y. Liu, J. Zhou, and T. F. Krauss, "Engineering gratings for light trapping in photovoltaics: The supercell concept," Phys. Rev. B **86**, 041404 (2012).
21. T. K. Chong, J. Wilson, S. Mokkapati, and K. R. Catchpole, "Optimal wavelength scale diffraction gratings for light trapping in solar cells," Journal of Optics **14**, 024012 (2012).
22. E. R. Martins, J. Li, Y. Liu, V. Depauw, Z. Chen, J. Zhou, and T. F. Krauss, "Deterministic quasi-random nanostructures for photon control," Nat. Commun. **4**, 1–7 (2013).
23. K. Vynck, M. Burresi, F. Riboli, and D. S. Wiersma, "Photon management in two-dimensional disordered media," Nat. Mat. **11**, 1017–1022 (2012).
24. C. Lin, N. Huang, and M. L. Povinelli, "Effect of aperiodicity on the broadband reflection of silicon nanorod structures for photovoltaics," Opt. Express **20**, A125–A132 (2012).
25. P. Kowalczewski, M. Liscidini, and L. C. Andreani, "Engineering gaussian disorder at rough interfaces for light trapping in thin-film solar cells," Opt. Lett. **37**, 4868–4870 (2012).
26. D. Gerace and L. C. Andreani, "Disorder-induced losses in photonic crystal waveguides with line defects," Opt. Lett. **29**, 1897–1899 (2004).
27. M. Peters, C. Battaglia, K. Forberich, B. Bläsi, N. Sahraei, and A. Aberle, "Comparison between periodic and stochastic parabolic light trapping structures for thin-film microcrystalline silicon solar cells," Opt. Express **20**, 29488–29499 (2012).
28. P. Kowalczewski, M. Liscidini, and L. C. Andreani, "Light trapping in thin-film solar cells with randomly rough and hybrid textures," Opt. Express **21**, A808–A820 (2013).
29. M. Burresi, F. Pratesi, K. Vynck, M. Prasciolu, M. Tormen, and D. S. Wiersma, "Two-dimensional disorder for broadband, omnidirectional and polarization-insensitive absorption," Opt. Express **21**, A268–A275 (2013).
30. F. Pratesi, M. Burresi, F. Riboli, K. Vynck, and D. S. Wiersma, "Disordered photonic structures for light harvesting in solar cells," Opt. Express **21**, A460–A468 (2013).
31. A. Herman, C. Trompoukis, V. Depauw, O. El Daif, and O. Deparis, "Influence of the pattern shape on the efficiency of front-side periodically patterned ultrathin crystalline silicon solar cells," J. Appl. Phys. **112**, 113107 (2012).
32. S. J. Jang, Y. M. Song, C. I. Yeo, C. Y. Park, J. S. Yu, and Y. T. Lee, "Antireflective property of thin film a-si solar cell structures with graded refractive index structure," Opt. Express **19**, A108–A117 (2011).
33. Y.-F. Huang, S. Chattopadhyay, Y.-J. Jen, C.-Y. Peng, T.-A. Liu, Y.-K. Hsu, C.-L. Pan, H.-C. Lo, C.-H. Hsu, Y.-H. Chang, C.-S. Lee, K.-H. Chen, and L.-C. Chen, "Improved broadband and quasi-omnidirectional anti-reflection properties with biomimetic silicon nanostructures," Nature Nanotechnology **2**, 770–774 (2007).
34. S. Y. Chou, P. R. Krauss, and P. J. Renstrom, "Imprint of sub-25 nm vias and trenches in polymers," Appl. Phys. Lett. **67**, 3114–3116 (1995).
35. J. Frühauf, *Shape and Functional Elements of the Bulk Silicon Microtechnique: A Manual of Wet-Etched Silicon Structures* (Springer-Verlag, 2005).
36. D. Lockau, T. Sontheimer, C. Becker, E. Rudigier-Voigt, F. Schmidt, and B. Rech, "Nanophotonic light trapping in 3-dimensional thin-film silicon architectures," Opt. Express **21**, A42–A52 (2013).

#235598 - $15.00 USD Received 4 Mar 2015; revised 22 Apr 2015; accepted 26 Apr 2015; published 15 May 2015

37. J. Gjessing, E. S. Marstein, and A. Sudbø, "2D back-side diffraction grating for improved light trapping in thin silicon solar cells," Opt. Express **18**, 5481–5495 (2010).
38. O. Sigmund and K. Hougaard, "Geometric properties of optimal photonic crystals," Phys. Rev. Lett. **100**, 153904 (2008).
39. B. C. P. Sturmberg, K. B. Dossou, L. C. Botten, A. A. Asatryan, C. G. Poulton, R. C. McPhedran, and C. M. de Sterke, "Absorption enhancing proximity effects in aperiodic nanowire arrays," Opt. Express **21**, A964–A969 (2013).
40. C. S. Schuster, A. Bozzola, L. C. Andreani, and T. F. Krauss, "How to assess light trapping structures versus a Lambertian Scatterer for solar cells?" Opt. Express **22**, A542–A551 (2014).
41. S. E. Han and G. Chen, "Toward the Lambertian Limit of light trapping in thin nanostructured silicon solar cells," Nano Lett. **10**, 4692–4696 (2010).
42. European photoNvoltaic project, `http://www.photonvoltaics.org/` (2015). [This project has received funding from the European Union's Seventh Framework Programme for research, technological development and demonstration under grant agreement No 309127, PhotoNVoltaics].
43. V. Depauw, Y. Qiu, K. Van Nieuwenhuysen, I. Gordon, and J. Poortmans, "Epitaxy-free monocrystalline silicon thin film: first steps beyond proof-of-concept solar cells," Prog. Photovolt. Res. Appl. **19**, 844–850 (2011).
44. American Society for Testing Materials , http://rredc.nrel.gov/solar/spectra/am1.5/. (2015).
45. K.-H. Brenner, "Aspects for calculating local absorption with the rigorous coupled-wave method," Opt. Express **18**, 10369–10376 (2010).
46. R. Judson, "Genetic algorithms and their use in chemistry," in *Reviews in Computational Chemistry* (John Wiley & Sons, Inc., 1996), pp. 1–73.
47. A. Lin and J. Phillips, "Optimization of random diffraction gratings in thin-film solar cells using genetic algorithms," Sol. Energy Mater. Sol. Cells **92**, 1689–1696 (2008).
48. A. Mayer, L. Gaouyat, D. Nicolay, T. Carletti, and O. Deparis, "Multi-objective genetic algorithm for the optimization of a flat-plate solar thermal collector," Opt. Express **22**, A1641–A1649 (2014).
49. R. L. Haupt and D. H. Werner, *Genetic Algorithms in Electromagnetics* (Wiley-IEEE Press, 2007).
50. A. Mayer and A. Bay, "Optimization by a genetic algorithm of the light-extraction efficiency of a GaN light-emitting diode," J. Opt. **17**, 025002 (2015).
51. A. Deinega, I. Valuev, B. Potapkin, and Y. Lozovik, "Minimizing light reflection from dielectric textured surfaces," J. Opt. Soc. Am. A **28**, 770–777 (2011).
52. J. Springer, A. Poruba, L. Müllerova, M. Vanecek, O. Kluth, and B. Rech, "Absorption loss at nanorough silver back reflector of thin-film silicon solar cells," J. Appl. Phys. **95**, 1427–1429 (2004).
53. F.-J. Haug, T. Söderström, O. Cubero, V. Terrazzoni-Daudrix, and C. Ballif, "Plasmonic absorption in textured silver back reflectors of thin film solar cells," J. Appl. Phys. **104**, 064509 (2008).
54. C. Trompoukis, I. Abdo, R. Cariou, I. Cosme, W. Chen, O. Deparis, A. Dmitriev, E. Drouard, M. Foldyna, E. G. Caurel, I. Gordon, B. Heidari, A. Herman, L. Lalouat, K.-D. Lee, J. Liu, K. Lodewijks, F. Mandorlo, I. Massiot, A. Mayer, V. Mijkovic, J. Muller, R. Orobtchouk, G. Poulain, P. Prod'Homme, P. R. i. Cabarrocas, C. Seassal, J. Poortmans, R. Mertens, O. E. Daif, and V. Depauw, "Photonic nanostructures for advanced light trapping in thin crystalline silicon solar cells," Phys. Status Solidi A **212**, 140–155 (2015).

## 1. Introduction

The photovoltaic (PV) market is dominated by technologies based on silicon [1]. Nowadays, crystalline silicon (c-Si) represents 87% of the PV market [2]. The major reasons for this supremacy are that c-Si is abundant, stable, non-toxic and absorbs the majority of the solar spectrum, up to $1.2\mu$m. Ten years ago, the price of Si material was much higher than today. In 2001, 70% of the module cost came from the material [3]. Nowadays, this proportion has decreased down to about 20% [4]. In spite of the fact that going to thinner films is no more a priority from the point of view of PV cost reduction, it is still relevant to get higher efficiency using less material, both scientifically and environmentally speaking. The use of ultrathin c-Si films is a well-known solution to achieve this goal [5, 6]. However, an obvious problem is associated with ultrathin films: a significant reduction of the absorption occurs if the film thickness is lower than the absorption length of the material, which is a major efficiency limiting factor. To overcome this issue, some techniques help keeping a high efficiency. For example, nano-texturing of the front-side and/or back-side surfaces of the solar cell allows to enhance the coupling of the incident light into the active layer via light trapping [7, 8]. Attention is paid to the optimization of this type of texture and a lot of simulations and experimental results on

#235598 - $15.00 USD Received 4 Mar 2015; revised 22 Apr 2015; accepted 26 Apr 2015; published 15 May 2015

nanostructured solar cells have been published in the last few years [9–13]. In spite of all these efforts, an important question has not yet found a definite answer: Is the best type of corrugation periodic, quasi-periodic or random? [14, 15].

The study of disordered structures is of high interest since it is easier to fabricate structures that are not perfectly ordered, tolerances on structured features being much more relaxed in this case [16]. Furthermore, partially disordered structures reduce the sensitivity to light polarization and incidence angle [17]. The major difference between periodic and random structures is that the former excite a well-defined Fourier spectrum, coupling light only at specific wavelengths. On the contrary, disordered structures have a richer Fourier spectrum, increasing the number of accessible diffraction orders and therefore the density of photonic states [18–20]. This property improves the coupling of the incident radiation into a broad spectral range thanks to scattering in various directions [14, 19–22]. Indeed, ordered structures lead to sharp peaks in the absorption spectrum due to the presence of coherent resonant Bloch modes. With the introduction of disorder, the modes overlap and the peaks tend to fade away, leading to a smoothing of the absorption spectrum [18]. The absorption at a specific wavelength decreases, but it increases at other wavelengths, leading to a broader and more uniform absorption spectrum.

Finding the optimal level of disorder into a structure is tricky. Recent studies have shown that the optimal structure is neither perfectly ordered nor totally random but a combination of both types [19, 20, 23, 24]. For this purpose, the inclusion of a controlled Gaussian disorder is an interesting approach [19, 25, 26]. The use of a binary search algorithm was also suggested by Martins and co-workers [20]. This algorithm allows them to find the appropriate level of disorder into a structure by tuning its Fourier spectrum. Researches were carried out on random rough interfaces [14, 22, 25, 27, 28], disordered cylindrical holes [17, 18, 23, 26, 29, 30] or disordered gratings [19–21]. In the present study, we focus on hole patterns made of inverted nano-pyramids. Due to the incremental adaptation of the refractive index [31–33], the pyramidal hole shape allows efficient antireflection to take place. More specifically, we focus on a fair numerical comparison between a technologically realizable correlated disorder pattern of inverted pyramids in an ultrathin c-Si layer, and its periodically patterned counterpart (same hole filling fraction, hole shape, etc.). The c-Si active layer is integrated into a realistic yet simplified solar cell architecture (anti-reflective layer, back reflector). We discard the parasitic absorption by taking only into account the absorption of the active layer. To be as realistic as possible, we chose existing lithography techniques as references, namely the Hole-mask Colloidal Lithography (HCL) [16] and the Nano-Imprint Lithography (NIL) [34], in order to produce correlated-disorder and periodic patterns respectively. Regarding the etching technology, the wet chemical etching was chosen to provide inverted nano-pyramidal holes [35]. Based on numerical simulations, we show that correlated-disorder inverted nano-pyramids provide typically greater efficiency than their periodic counterparts. The hole filling fraction plays the dominant role, regardless of the fact that the structure is periodic or not. This conclusion is similar to those reported for cylindrical holes [23] and 1D gratings [19]. However, we predict that the benefits of correlated disorder are limited by the maximal filling fraction achievable with present patterning technologies.

## 2. Methodology

The most common nanostructures for light-trapping are periodic [9, 31, 36–38]. Periodic structures are typically defined by the period ($P_{UC}$) of the unit cell ($UC$), the filling fraction of air holes into the active material ($f_{UC}$) and the shape of the holes, for example, the width of inverted pyramids ($W_{UC}$) (cf. Fig. 1(a)). Periodic structures have to be optimized to find the best efficiency. Pseudo-random structures can improve the efficiency in comparison to periodic ones. Modeling such structures requires the use of a super-cell period ($P_{SC}$) in order to emulate

#235598 - $15.00 USD Received 4 Mar 2015; revised 22 Apr 2015; accepted 26 Apr 2015; published 15 May 2015

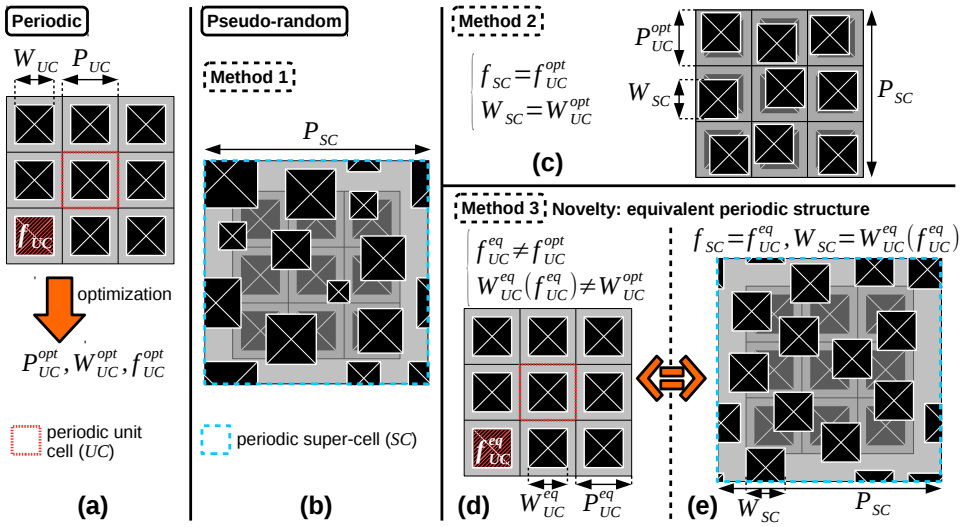


Fig. 1. Methods for introducing disorder into a periodic structure. (a) Periodic structure defined by unit cell ($UC$), period ($P_{UC}$), hole shape and size (here an inverted pyramid of width $W_{UC}$) and hole filling fraction ($f_{UC}$). $P_{UC}^{op}$, $W_{UC}^{op}$ and $f_{UC}^{op}$ are optimal parameters for the best efficiency. (b) Most general method to model a pseudo-random structure defined by super-cell ($SC$), user-set period ($P_{SC}$), hole shape, hole size (which may vary among holes), hole positions (random or correlated disorder) and filling fraction ($f_{SC}$). (c) Second method to introduce randomness by keeping the same parameters as for the optimal periodic structure (cf. (a)) and by varying the hole positions only. (d-e) Third method to introduce randomness. The equivalent periodic unit cell (d) is taken as a reference; its filling fraction $f_{UC}^{eq}$ is set by the user whereas other structure parameters ($P_{UC}^{eq}$ and $W_{UC}^{eq}$) are obtained by optimization. The pseudo-random super-cell (e) is defined by keeping the equivalent periodic structure parameters ($f_{UC}^{eq}$ and $W_{UC}^{eq}$) while changing randomly the hole positions.

the disorder [19,20]. In general, in comparison with the optimized periodic structure, a pseudo-random structure may have a different filling fraction and different positions and widths of holes (Fig. 1(b)). This type of general pseudo-random structure has already been studied [19, 20].

An alternative method also exists in order to introduce disorder into a periodic structure (Fig. 1(c)). This method consists in keeping both the filling fraction and the width constant (i.e. the same as those of the optimal periodic unit cell). The disorder is introduced by changing the hole positions only [18, 39]. However, in both previous methods, no comparison with an *equivalent* periodically patterned structure was reported so far. In this work, the equivalent periodic structure (Fig. 1(d)) is defined by the equivalent period ($P_{UC}^{eq}$) of the unit cell and the equivalent hole width ($W_{UC}^{eq}$). For a given filling fraction $f_{UC}^{eq}$ chosen by the user, both parameters ($P_{UC}^{eq}$ and $W_{UC}^{eq}$) are optimal (i.e. they provide the best solar cell efficiency). The method we use for introducing randomness consists in keeping the hole width constant, changing the hole filling fraction and randomly setting the hole positions (Fig. 1(e)). This method was used already by several groups [17, 23, 29, 30]. However, unlike in these studies which often use a planar reference, we introduce here the use of an equivalent periodic structure for comparison. Indeed, since the filling fraction is allowed to change, the comparison with the optimal periodic unit cell ($P_{UC}^{op}$, $W_{UC}^{op}$, $f_{UC}^{op}$) is not fair because the quantity of material in the pseudo-random cell and the periodic cell is not the same. Therefore, the use of equivalent periodic structures (i.e.

#235598 - $15.00 USD Received 4 Mar 2015; revised 22 Apr 2015; accepted 26 Apr 2015; published 15 May 2015

defined by keeping the same filling fraction for both periodic and pseudo-random structures: $f_{SC} = f_{UC}^{eq}$), allows us to perform, for the first time, a fair comparison between pseudo-random and periodic structures.

Recently, the concept of light trapping efficiency was proposed by Schuster and coworkers in order to compare, on the basis of an ideal Lambertian scatterer, structures that vary greatly between each other in terms of local and global geometries, and active materials [40]. In principle, it could have been applied to our study, as well. However, since we deal with structures made from the same local geometry (inverted pyramid) on the same material (c-Si) but having only different patterns (periodic and correlated disorder), it was more pertinent in our case to compare directly both types of structure, provided an equivalent periodic counterpart was defined that allowed a fair comparison. Our methodology, though restricted to the present case, simplifies the comparison since it does not require the use of a Lambertian reference.

We note that scattering properties of light trapping structures have been recognized to be mainly determined by local geometrical features [15,41]. In our study, we chose inverted pyramids as a realistic feature (easy to fabricate in silicon by wet etching) and took them as building blocks of both periodic and correlated disorder structures. Besides these aspects, our approach brings the following novelty: 1) correlated disorder structures are directly compared with their periodic equivalent counterparts, 2) the super-cell concept combined with RCWA allows us to treat both periodic and correlated disorder structures on equal footing, which enables straightforward comparison.

### *2.1. Studied structures*

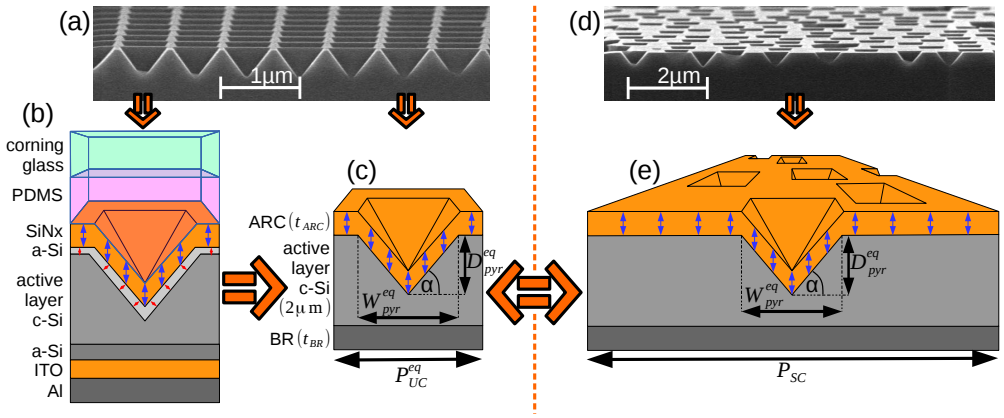


Fig. 2. Studied structures. (a) SEM image of periodically patterned c-Si wafer (NIL and wet etching processes), (b) schematic view example of realistic solar cell, (c) simplified periodic solar cell studied in this work, (d) SEM image of randomly patterned c-Si wafer (HCL and wet etching processes), (e) simplified pseudo-random solar cell studied in this work. Note that a fair comparison between pseudo-random and equivalent periodic solar cells requires the use of the same structure parameters (hole size and shape, layer thicknesses) in both cases.

The structures under study are based on crystalline silicon thin film technology. An example of a realistic solar cell investigated in the PhotoNVoltaics project [42] and based on heterojunction IBC (Interdigitated Back-Contact) cell technology is shown in Fig. 2(b). Considering the main purpose of our study, we focused on simplified structures as shown in Fig. 2(c) and 2(e).

In the equivalent periodic structure (Fig. 2(c)), the c-Si thickness is set to 2 $\mu$m, for reasons

#235598 - $15.00 USD Received 4 Mar 2015; revised 22 Apr 2015; accepted 26 Apr 2015; published 15 May 2015

briefly explained hereafter. Ultrathin c-Si films can be fabricated by dedicated processes only, such as Epifree [43]. This technique is based on the reorganization upon annealing at high temperature of cylindrical macropore arrays in silicon. At high temperature, macropores merge to form a wide plate-like void. Under this plate, a detachable perfect micron-thin film is formed. This film is then lifted off and leads to a high-quality monocrystalline thin-film. By modifying the macropore array dimensions, it is possible to control the thickness. Typical thicknesses vary from 1 to 5 $\mu$m.

The front side of the active layer is then textured with a periodic square array of inverted pyramidal holes. The width of the pyramidal hole ($W_p^{eq}$) and the pitch of the pattern (i.e. the period of the unit cell $P_{UC}^{eq}$) are variable parameters. Period and hole width are related together by the hole filling fraction: $f_{UC}^{eq} = (W_p^{eq}/P_{UC}^{eq})^2$. The angle ($\alpha$) between the pyramid side and the horizontal axis has a fixed value of $\alpha = 54.7°$, which results from preferential etching of c-Si along the $\{111\}$ cristallographic direction [35]. Both $W_p^{eq}$ and $\alpha$ determine the depth ($D_p^{eq}$) of the inverted-pyramid: $D_p^{eq} = W_p^{eq}/2\tan\alpha$. The top of the c-Si active layer is coated with a conformal ITO anti-reflective layer (ARC). The active layer is placed on a back-reflector (BR) made of Aluminium (Al). The thicknesses of the ARC and Al layers are constant and fixed according to the optimization process described in section 3.1.

In the pseudo-random structure (Fig. 2(e)), the inverted-pyramid parameters ($W_p^{eq}$, $D_p^{eq}$ and $\alpha$) and the three layer thicknesses (ITO, c-Si and Al) are exactly the same as the parameters of the equivalent periodic structure. The positions of the holes are set randomly by respecting (if possible) the pinning distance, i.e. the distance between two neighboring holes, in order to mimic texturing obtained by HCL process [16] (more details can be found in subsection 3.3).

### 2.2. *Calculation of the short circuit current*

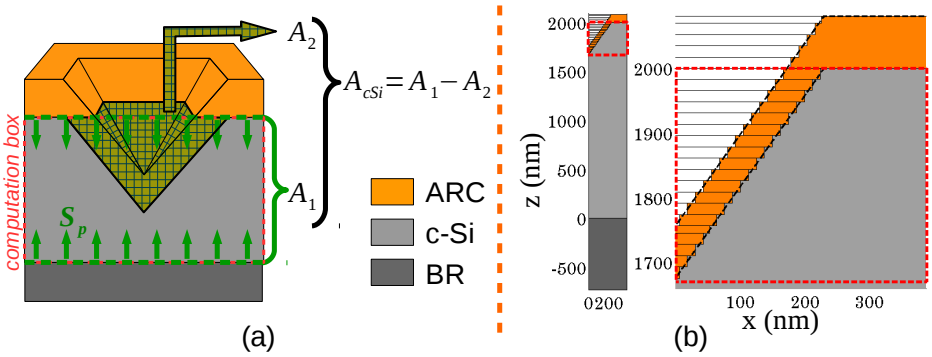


Fig. 3. (a) Computation of the absorption in the active layer of a solar cell. $A_1$: absorption between both two horizontal planes (*computation box*) obtained by computing Poynting vectors $S_p$ along these planes. $A_2$: parasitic absorption in the ARC layer obtained by computing the local absorption in the ARC volume. $A_{cSi} = A_1 - A_2$: absorption in the active c-Si layer. (b) Vertical discretization of the structure in the computation box.

Solar cells are characterized by computing the short circuit current:

$$J_{sc} = \frac{e}{hc}\int_{350nm}^{1100nm} S(\lambda)A_{cSi}(\lambda)\lambda d\lambda, \tag{1}$$

where $e$ is electron charge, $h$ is the Planck constant, $c$ is the speed of light in vacuum, $\lambda$ is the wavelength, $S(\lambda)$ is the air mass (AM1.5G) solar spectrum [44] and $A_{cSi}(\lambda)$ is the absorption

#235598 - $15.00 USD Received 4 Mar 2015; revised 22 Apr 2015; accepted 26 Apr 2015; published 15 May 2015

spectrum inside the c-Si active layer. The integration is performed within the wavelength range where photons are absorbed by the c-Si. Computation is done for 80 wavelengths with a variable step in order to refine the spectrum at long wavelengths ($\lambda > 700$ nm), where light trapping into quasi-guided modes takes place. For each wavelength, the absorption inside the active layer is calculated by using an original hybrid method based on Rigorous Coupled-Wave Analysis (RCWA) method (see Fig. 3). The calculation procedure comprises three steps. (1) Two horizontal planes are defined to hold the entire volume of the c-Si active layer. The area between the two planes is called the *computation box*. These planes are spatially discretized ($\Delta_i = 5$ nm, $i = \{x,y\}$) and the component of the Poynting vector normal to the planes is computed by RCWA at each point. Poynting vector components are spatially integrated in order to calculate the energy flow through both planes. From these flows, we calculate the energy absorbed by all materials in the computation box (basically, the Poynting vector computation has to be done all around the computation box, but considering the periodicity of the cell, computation along the vertical walls, i.e. along the periodic boundaries, is useless.). (2) The second step consists in the computation of the parasitic absorption in the computation box (in the present case, the parasitic absorption takes place in the ARC since the BR layer is excluded from the computation box). The ARC area in the computation box is spatially discretized ($\Delta_i = 5$ nm, $i = \{x,y,z\}$) and the local absorption is computed by RCWA [45] at each point of the mesh and then spatially integrated in order to evaluate the parasitic absorption. (3) The absorption in the active layer is defined by the absorption in the whole computation box (step 1) minus the parasitic absorption (step 2). Once the absorption spectrum in the active layer is calculated, it is interpolated on a finely resolved grid (constant wavelength step of 0.5 nm) by using a cubic interpolation method. The AM 1.5 solar spectrum is also interpolated with the same step. To determine $J_{sc}$, the integral (eq. 1) is numerically computed using the trapeze method.

## 3. Results and discussion

The efficiency of equivalent periodic structures and pseudo-random structures is computed (see subsection 2.1), from which a fair comparison between both structures is performed.

### *3.1. Optimal periodic structure*

**Table** 1. **GA parameters (top) and optimal structure parameters provided by the GA (bottom).**

| | Parameter | Value |
|---|---|---|
| GA para. | size of population | 100 |
| | number of generations | 100 |
| | rate of crossover (%) | 90 |
| | rate of mutation (‰) | 5 |
| structure para. | $P_{UC}^{opt}$ (nm) | 623 |
| | $f_{UC}^{opt}$ (%) | 94 |
| | $t_{ARC}^{opt}$ (nm) | 82 |
| | $t_{BR}^{opt}$ (nm) | 729 |
| | $J_{sc}^{opt}$ (mA·cm$^{-2}$) | 24.3 |

The first step consists in performing a full optimization of the periodic (wet chemical etched) solar cell (Fig. 2(c)). Four parameters have to be optimized: the period $P_{UC}$ of the unit cell which corresponds to the pitch of the pattern, the filling fraction $f_{UC}$ of the holes at the top c-Si surface, and the thicknesses of the ARC and BR layers, respectively $t_{ARC}$ and $t_{BR}$. The optimization of these parameters was performed by a Genetic Algorithm (GA) method [46–49]

#235598 - $15.00 USD Received 4 Mar 2015; revised 22 Apr 2015; accepted 26 Apr 2015; published 15 May 2015

thanks to a home-made code (see [50] for details). The idea consists in working with a population of 100 individuals, each individual being representative of a given set of parameters which are actually represented by a string of binary digits (DNA). We select by a rank-based roulette wheel selection 50 parents for the next generation. For any pair of parents, two children are determined either by a one-point crossover of the parents' DNA (90% probability) or by a simple replication of the parents (10% probability). In addition, each bit of the children's DNA has a probability of 0.5% to be reversed (random mutations). Elitism is finally implemented in order to make sure that the best solution is not lost. When repeated from generation to generation (maximum of 100 generations), this evolutionary strategy leads to the global optimum of $J_{sc}$. The advantage of using a GA approach is that it is not necessary to scan all possible parameter combinations, which leads to a huge gain in computational time. The strategic parameters of the GA as well as the solution provided by this approach are listed in Table 1.

**Table** 2. **Evolution of $J_{sc}$ and computation time with the number of wavelength points. Variable wavelength step and interpolation were used for the 80-points case. Constant step was used in all other cases.**

| Number of $\lambda$ points | 80 | 100 | 200 |
|---|---|---|---|
| $J_{sc}$ (mA·cm$^{-2}$) | 24.30 | 24.11 | 24.14 |
| computation time (hours) | 1 | 1.3 | 2.7 |
| Number of $\lambda$ points | 500 | 1000 | 2000 |
| $J_{sc}$ (mA·cm$^{-2}$) | 24.16 | 24.18 | 24.20 |
| computation time (hours) | 6.7 | 13.3 | 26.6 |

Regarding the RCWA computation accuracy, $7 \times 7$ diffraction orders where taken into account and the spatial steps of the mesh were set at 5 nm in each direction. The optimal structure parameters provided by the GA and the corresponding short-circuit current $J_{sc}^{opt}$ are listed in Table 1. As explained in subsection 2.2, computation of the absorption spectrum is done for 80 wavelength points with a variable step, i.e. 20 points for $\lambda < 700$ nm and 60 points for $\lambda > 700$ nm. In order to validate such a discretization scheme, several simulations were performed for the same optimized structure by varying the number of wavelength points. The corresponding $J_{sc}$ values and computation times are listed in Table 2. If we compare the $J_{sc}$ values for 80 points and 2000 points, the latter being considered as the exact (converged) value, the estimated relative error is $\pm 0.4\%$. Therefore, we can safely conclude that the use of 80 points (with variable step and interpolation) is sufficient to provide a reliable $J_{sc}$ estimation. Moreover, this method allows a drastic reduction of the computation time.

The absorption spectrum in each layers is shown in Fig. 4. We found an optimal pitch $P_{UC}^{opt}$ equal to 623 nm. Physically, this optimum results from a trade-off between light in-coupling and out-coupling into/from quasi guided diffraction modes and is typical of what can be found in literature [15,31,41,51]. A general trend is that the optimal pitch should be of the order of the average wavelength between free space and silicon [51]. We notice that the best $J_{sc}$ corresponds to the highest filling fraction allowed in GA computation (95%). This result is in accordance with the need for a small amount of flat surface on c-Si front side [31, 51], but it represents a real challenge for the fabrication process.

We notice that high parasitic absorption takes place at long wavelengths in the Al back reflector due to the excitation of surface plasmon polaritons [52, 53]. In order to reduce this parasitic absorption, real devices include a buffer layer of transparent conductive oxide, such as ITO, between the active layer and the back reflector (Fig. 2(b)). The studied structure (Fig. 2(c)) does not include the buffer ITO layer because it was not essential for the comparison between periodic and correlated disorder structures.

#235598 - $15.00 USD Received 4 Mar 2015; revised 22 Apr 2015; accepted 26 Apr 2015; published 15 May 2015

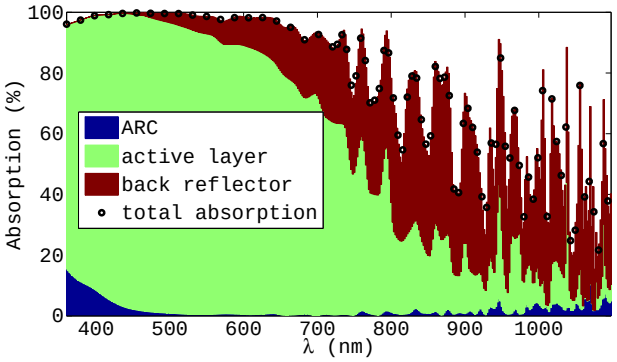


Fig. 4. Absorption spectrum in each layer of the optimal periodic structure determined by the GA.

### 3.2. *Equivalent periodic structures*

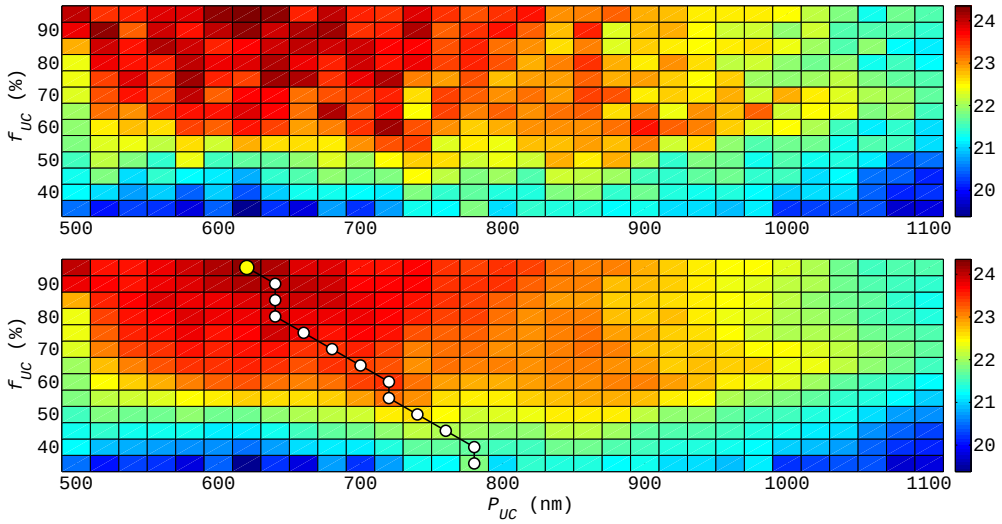


Fig. 5. $J_{sc}$ maps (mA·cm$^{-2}$) and determination of equivalent periodic structures for each filling fraction by scanning the period $P_{UC}$ of the unit cell: RCWA results (top) and smoothed RCWA results (bottom) by taking into account the experimental inaccuracies of NIL and wet etching processes. White circles represent the selected equivalent periodic structures and yellow circle is the optimal one (i.e. highest $J_{sc}$).

Previous simulations based on the genetic algorithm allowed us to determine the optimal parameters (i.e. providing the highest $J_{sc}$) for a periodic structure. As explained in section 2, the strategy of our method is to vary the filling fraction in order to observe the influence of this parameter on the efficiency of solar cells periodically or randomly patterned. For this purpose, 13 values of the filling fraction were considered between 35% and 95%, with a step of 5%. For a fair comparison, the periodic structure has to be optimized for each filling fraction value. Although the genetic algorithm seems to be the most appropriate method, a scan of parameters was used because of computational time considerations. For each filling fraction value, the

#235598 - $15.00 USD Received 4 Mar 2015; revised 22 Apr 2015; accepted 26 Apr 2015; published 15 May 2015

width of the pyramid $W_p$ (and therefore the period of the unit cell $P_{UC} = W_p/\sqrt{f_{UC}}$) was the only scanned parameter. The thicknesses of the ARC and BR layers were fixed (we used the same values as for the GA optimized periodic structure, see Table 1).

Maps of $J_{sc}$ are shown in Fig. 5. The top part of Fig. 5 gives the $J_{sc}$ directly obtained by RCWA by considering perfect NIL and wet etching processes, i.e. filling fraction and period matching prescribed values. According to experimental data [42], some inaccuracies can occur in the pattern fabrication, which are estimated to $\pm 5\%$ for the filling fraction and to $\pm 5$ nm for the period. These error margins are taken into account in the smoothed map of $J_{sc}$ (bottom part of Fig. 5). The selection of equivalent periodic structures is based on this smoothed map: for each filling fraction value, i.e. each horizontal line of the map, the equivalent period $P_{UC}^{eq}$ is determined by the highest $J_{sc}$ on the line (white circle). We note that the equivalent period at $f_{UC}^{eq} = 95\%$ (yellow circle) corresponds to the optimal period given by the GA (see Table 1).

### *3.3. Pseudo-random structures*

Pseudo-random structures are defined by keeping the same parameters as for the equivalent periodic structures (see Fig. 2(e)). The inverted pyramids are positioned randomly on the front side of the active layer. Since the RCWA method only deals with periodic structures, the use of a super-cell is required. The super-cell approach [18, 20, 22] consists in periodically repeating a finite disordered cell.

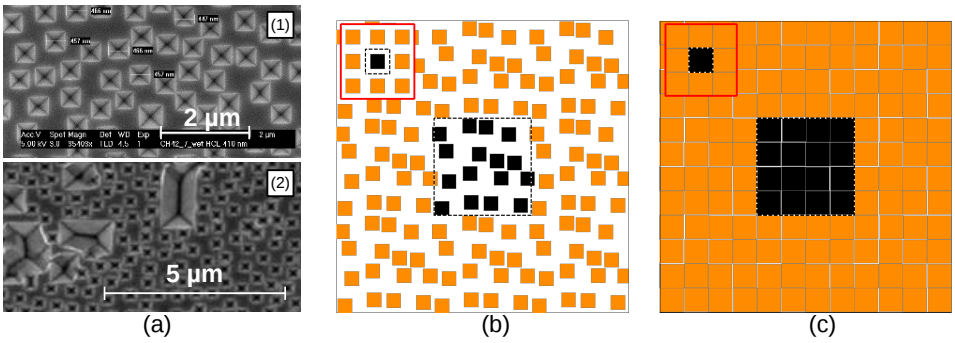


Fig. 6. Random hole positions. (a) SEM top view images of c-Si wafer patterned by HCL and wet etching with non overlapping holes (top) and some overlapping holes (down). (b-c) Top views of super-cells for two different filling fractions ($f_{SC} = 35\%$ and $f_{SC} = 95\%$ respectively). Black square holes belong to the super-cell modeled by RCWA. Orange square holes belong to neighboring super-cells. In the red frame (upper left corner), the equivalent periodic cell is shown for comparison.

Here, the super-cell is defined by three parameters: the number of holes $N_{holes}$ in the super-cell, the hole filling fraction $f_{SC}$ and the (pseudo-)period $P_{SC}$. The number of holes is chosen to mimic the pseudo-random pattern of a realistic structure. The filling fraction is the only variable. The super-cell period is directly obtained from $N_{holes}$, $f_{SC}$ and $W_p^{eq}$, according to $f_{SC} = N_{holes}\left(W_p^{eq}/P_{SC}\right)^2$. Note that holes are not allowed to overlap in the super-cell. According to experimental results, overlapping holes result in "giant" holes after wet etching and damage the light trapping efficiency (see Fig. 6(a)).

As explained previously, we attempt to mimic pseudo-random solar-cell patterns obtained by HCL and wet etching technologies. Although the hole size and shape are defined by the wet etching step, the positions of holes are set by the HCL step and result from the self-assembly of surface-charged polystyrene beads over the c-Si surface [16, 54]. The HCL method imposes

#235598 - $15.00 USD Received 4 Mar 2015; revised 22 Apr 2015; accepted 26 Apr 2015; published 15 May 2015

a minimal distance between two beads (and therefore between to holes after etching). Such pinning distance is estimated to be about twice the bead diameter. In this work, beads that were two times smaller than the desired hole width were used. This allows bead positioning to be as free as possible. Then, for each desired hole width (i.e. each filling fraction), a new bead size was used.

Examples of super-cells for two different filling fractions are shown in Figures 6(b) and 6(c). The case of a low filling fraction is representative of a real solar cell obtained by HCL. High filling fraction HCL patterns (like in Fig. 6(c)) are still unrealistic due to experimental restrictions. Considering recent experimental studies [42], the filling fraction upper limit is estimated to be approximately 55%. Hereafter, we choose to investigate a large range of filling fractions, up to 95%, while keeping in mind this experimental limit, in anticipation of future technological progresses.

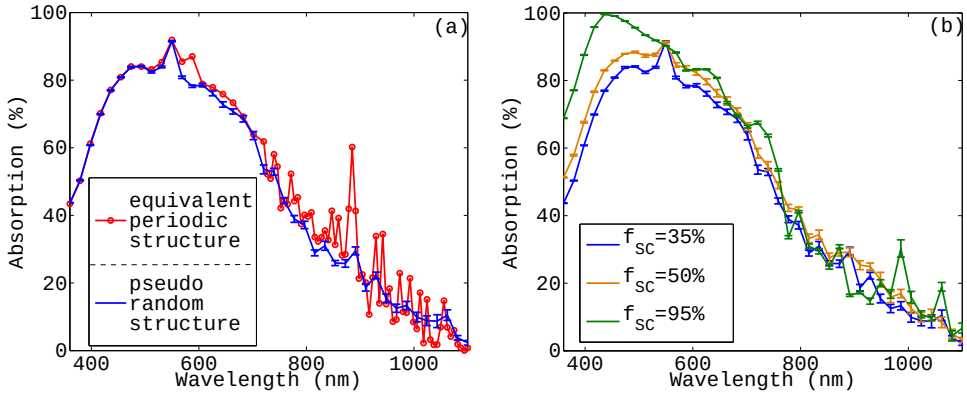


Fig. 7. (a) Absorption spectra of equivalent periodic solar cells (red circles) and pseudo-random solar cells (blue bars) for 35% filling fraction in both cases. (b) Evolution of the absorption spectrum with the filling fraction in pseudo-random solar cells.

To perform simulations of pseudo-random cells, the spatial step of the super-cell mesh (see section 2.2) is set to 5 nm, as for periodic structures. Considering the RCWA numerical accuracy and the large period of the super-cell compared to the hole size, $19 \times 19$ diffraction orders were taken into account in the RCWA calculations. In order to perform statistical studies (which are necessary because of the random character of the structure), 20 RCWA simulation runs were performed and their results were then averaged. Absorption spectra of different structures are shown in Fig. 7. In Fig. 7(a), a comparison between pseudo-random and equivalent periodic structures is performed for a filling fraction of 35%. Both absorption spectra are similar at short wavelengths (lower than 600 nm). Differences appear at wavelengths longer than 700 nm due to interferences that take place in periodic cells only. The spectrum of the pseudo-random structure is smoothed due to the randomness of the pattern. Nevertheless, according to Fig. 7(b), interferences could appear at high filling fraction in pseudo-random cells as well. Such a result is mainly due to the difficulty of modeling a random pattern with almost touching and non-overlapping square holes (Fig. 6(c)). In this case, the pseudo-random pattern is actually close to a periodic one.

### *3.4. Fair comparison between pseudo-random and equivalent periodic structures*

The comparison of $J_{sc}$ between pseudo-random and equivalent periodic structures, at each filling fraction, is shown in Fig. 8. Two curves pertain to the equivalent periodic structures: the first

#235598 - $15.00 USD Received 4 Mar 2015; revised 22 Apr 2015; accepted 26 Apr 2015; published 15 May 2015

one (red circles) is the initial RCWA result and the second one (blue squares) is the smoothed RCWA result taking into account experimental inaccuracies, as explained previously. As expected, the latter values are smoothed, due to the account of slight randomness in hole size and period during NIL and wet etching processes. We note also a drop in both curves (red circles, blue squares) around a filling fraction of 60%. The third curve (black line with error bars) is the average result of pseudo-random structures. The curve is relatively smooth due to the random character of the pattern. Moreover, as for the periodic case, the curve shows saturation behavior at filling fractions greater than 65%.

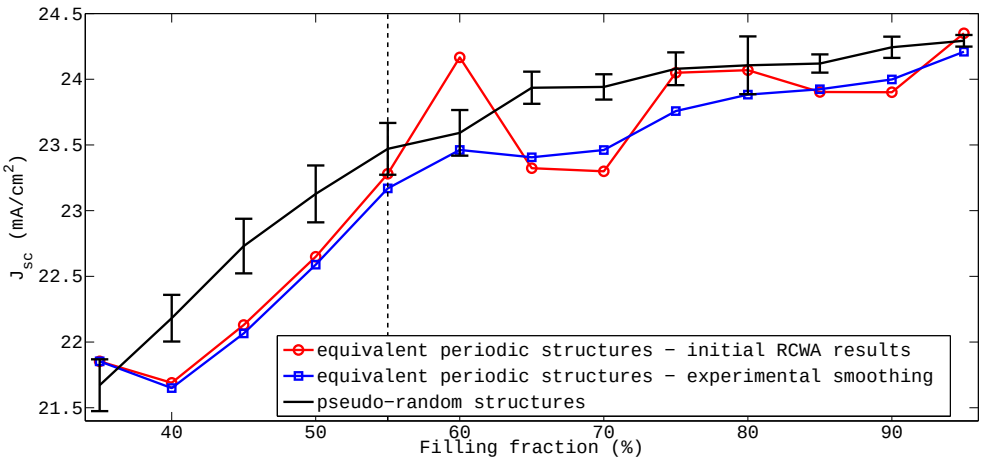


Fig. 8. Comparison of *Jsc* between pseudo-random and equivalent periodic solar cells. The vertical black dashed line denotes the maximal filling fraction reachable by HCL.

Comparing pseudo-random and equivalent periodic structures, the $J_{sc}$ of the pseudo-random structures is globally higher than the $J_{sc}$ of the equivalent periodic ones, whatever the filling fraction is. However, the difference between periodic and pseudo-random cases tends to be less pronounced as the filling fraction increases above 70%. It can be explained by the reduction of the randomness imposed by the positioning of holes in the super-cell (Fig. 6(c)), which leads to the decrease of the standard deviation (error bars) at high filling fraction values.

In overall, it can be concluded that pseudo-random structures always provide the best $J_{sc}$ whatever the filling fraction is. However, two other aspects have to be taken into account. The first one is related to experimental limitations of the studied technologies. Although these limitations have already been considered for periodic patterns, especially regarding the inaccuracies related to the imprinting (NIL) and the etching (wet) processes [42], similar limitations have still to be considered for pseudo-random patterns obtained by HCL. Indeed, one has to avoid overlapping holes when imprinting randomly inverted nano-pyramids by HCL and wet etching (Fig. 6(a)). As a result, the maximal filling fraction is necessarily restricted to about 55% according to experimental measurements. This sets a limit to $J_{sc}$ for pseudo-random patterns at $J_{sc} = 23.47 \pm 0.2$ mA/cm$^2$, to be compared with 24.21 mA/cm$^2$ achievable with optimal periodic pattern of filling fraction of 95%. In order to solve the problem of limited filling fraction for the HCL process, it is possible to couple it with dry plasma etching (instead of wet chemical etching) providing Gaussian-shaped holes. Indeed, such a method allows to have overlapping holes without forming "giant holes" and therefore to reach a filling fraction close to 95%. However, dry plasma etching causes a larger number of surface defects than wet etching, which will likely degrade the electrical performance of the devices. The second aspect is related to the cost of the different patterning technologies. Indeed, according to preliminary estimations of fabri-

#235598 - $15.00 USD Received 4 Mar 2015; revised 22 Apr 2015; accepted 26 Apr 2015; published 15 May 2015

cation costs [42], the NIL technology would be four times more expensive than the HCL one, which may be prohibitive in terms of the total cost of the solar cell. This consideration tends to favor the use pseudo-random rather than periodic patterns. On the other hand, new periodic patterning processes are currently under study, such as the LIL (Laser Interference Lithography) method which is less expensive than NIL, according to cost calculations made in the pNv project [42]

## 4. Conclusions

In summary, we performed a fair numerical comparison between realistic correlated-disorder inverted pyramids ultrathin c-Si textured films and their equivalent periodic counterparts, on the basis of their respective $J_{sc}$ for a large range of hole filling fractions. All parameters of modeled structures were set by respecting technological restrictions imposed by imprinting (NIL and HCL) and etching (wet chemical etching) processes. We showed that a correlated disorder patterned solar cell is more efficient than the equivalent periodic one, whatever the filling fraction is. However, the benefit decreases at high filling fractions. Considering the current technological constraints of the HCL process, the highest $J_{sc}$ achievable by HCL (filling fraction 55%) is slightly lower than the $J_{sc}$ of the optimal periodic structure provided by NIL (filling fraction 95%). But this issue could be solved by coupling the HCL process with dry plasma etching, allowing higher filling fractions. At present, the NIL technology is much more expensive than HCL, but less expensive imprinting processes such as LIL are worth to be investigated.

## Acknowledgments

All partners of PhotoNVoltaics project [42] are acknowledged for providing experimental data and optical constant data. This research used resources of the "Plateforme Technologique de Calcul Intensif (PTCI)" (http://www.ptci.unamur.be) located at the University of Namur, Belgium, which is supported by the F.R.S.-FNRS under the convention No. 2.4520.11. The PTCI is member of the "Consortium des Equipements de Calcul Intensif (CECI)" (http://www.ceci-hpc.be).